Progress In Electromagnetics Research M, Vol. 109, 125–136, 2022

Design of Circular Polarization Multiplexing Beam Splitter Based on Transmission Metasurface

Honggang Hao, Yihao Tang*, Sen Zheng, Xuehong Ran, and Wei Ruan*

Abstract—A circular polarization multiplexing metasurface beam splitter operating at 15 GHz with polarization conversion effect is proposed. The unit cell is formed by alternately stacking 4 layers of metal and 2 layers of dielectric substrates cascaded along the propagation direction, separated by air. The resonant phase of the unit cell can be changed by changing the size parameters of the two arms of the metal cross patch, and the phase coverage of nearly 360° can be achieved in the direction of the two orthogonal linear polarization components, while transmission coefficient is above 85%. The circular polarization geometric phase covering 360° can be achieved by rotating the metal patch. The polarization conversion of the circularly polarized wave can be realized by setting the phase difference of the two orthogonal linear polarization components to 180°, and the polarization conversion ratio (PCR) at the working frequency is greater than 90%. The simulation and test results show that when the circularly polarized electromagnetic wave is perpendicularly incident on the metasurface beam splitter, the transmitted wave is divided into two circularly polarized waves with different exit angles and orthogonal to the polarization direction of the incident wave. This work may provide new ideas for the integration and miniaturization of traditional beam splitting devices and have important application prospects in fields such as multiple input multiple output (MIMO) systems.

1. INTRODUCTION

The polarization beam splitter is a passive device that can separate components of different polarization modes in incident electromagnetic waves, which is widely used in optical equipment such as interferometers. In optical field, semi-transmissive mirrors or birefringent materials are often used to achieve beam splitting effects, but these methods are too difficult to apply to the microwave frequency band. The metasurface has unique properties that traditional dielectric materials do not have. It can flexibly control the characteristics of electromagnetic wave amplitude, phase, and polarization in the wavefront, which is widely used in orbital angular momentum (OAM) beam generation, radar cross-section reduction, and high-gain lens antennas [1–5]. It provides a new idea for the design of the beam splitter in the microwave frequency band.

The phase control methods of metasurfaces mainly include two types: resonance phase control [6–8] and geometric phase control (also known as Pancharatnam-Berry (PB) phase control) [9–11]. The resonant phase refers to the phase response of the metasurface unit cell structure at a specific resonant frequency. By changing the size parameters of the unit cell structure, a nearly 360° phase coverage can be obtained at the resonant frequency. In 2016, Liu et al. designed a 2-bit anisotropically encoded metasurface to independently encode different polarization directions through transmission phase control to achieve independent control of different linear polarization components in electromagnetic waves [12]. In 2020, Lv et al. designed a transmissive metasurface that worked in the terahertz frequency band

Received 4 January 2022, Accepted 22 March 2022, Scheduled 1 April 2022
* Corresponding author: Yihao Tang (1198100277@qq.com), Wei Ruan (ruanwei@cqupt.edu.cn).
The authors are with the College of Photoelectric Engineering, Chongqing University of Posts and Telecommunications, Chongqing 400065, China.

by controlling the structural parameters of the unit cell, and the beam splitting effect on the linear polarization component of the terahertz wave was achieved [13]. The geometric phase was achieved by rotating the metal structure of the metasurface unit cell to achieve a sudden change in phase. The value of the phase change is twice the rotation angle. It is widely used in abnormal reflections, energy focusing, vortex beams, etc. Some research progress has been made in the regulation of circularly polarized electromagnetic waves based on the above two control methods, but their phase responses to orthogonal circularly polarized waves are coupled together, which limits the degree of freedom of control to a certain extent [14, 15].

In this paper, we combine resonant phase and geometric phase [16–18] to design a structure with a circular resonant ring embedded with cross metal patches. By changing the structural parameters of the unit cell, the resonance phase can be controlled. For different linearly polarized incident waves, the unit cell has different phase and amplitude responses. The phase covers 360°, and the transmission coefficient exceeds 85%. The control of the geometric phase is achieved by rotating the cross metal patch. For circularly polarized incident waves of different rotation directions, when the unit cell rotates 180° around the z-axis, the phase of the left-handed circular polarization changes to 360°, and the right-handed circle polarization phase changes to −360°. The value of the change is twice the rotation angle. Based on the principle of electric field superposition, combined with resonance phase and geometric phase, the phase distribution of two orthogonal circularly polarized waves is decoupled, and the effect of beam splitting in different directions and angles is achieved. The results of simulation analysis and physical test are basically the same.

2. DESIGN OF UNIT CELL

The structure of the unit cell designed in this paper is shown in Figure 1. The unit cell consists of 2 layers of air-separated dielectric plates and 4 layers of metal patches. The metal patches include a resonance ring and a cross patch. The thickness of the metal layer is $h_c = 0.035\,\text{mm}$; the dielectric substrate is made of F4B, whose dielectric constant is $\varepsilon = 2.2$; and the loss tangent is 0.01. The thickness of each dielectric substrate is $h_s = 2\,\text{mm}$; the thickness of the air layer is $h_a = 2.4\,\text{mm}$; the radius of the resonance ring is $r = 7\,\text{mm}$; the width is $w = 0.3\,\text{mm}$; the horizontal axis length of the center cross is a_x; the vertical axis length is a_y; the width is $d = 1\,\text{mm}$; and the unit cell period is $p = 7\,\text{mm}$. Unit cells of different sizes have different phase and amplitude responses at a certain resonant frequency. The resonant frequency of the unit cell can be changed by changing the size parameters a_x and a_y. So the transmission phase and amplitude of the unit cell could be controlled by a_x and a_y.

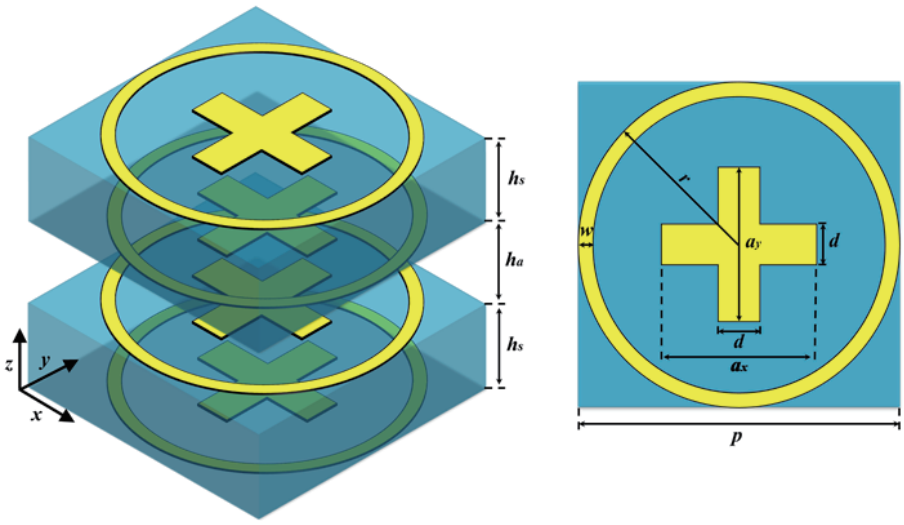

(a) (b)

Figure 1. (a) The 3D view of metasurface unit cell. (b) The top view of the metasurface unit cell.

The unit cell structure is shown in Figure 1. When the left-handed circularly polarized incident wave is incident perpendicular to the surface of the metasurface unit cell, the incident wave $\overrightarrow{E_+^{in}}$ and the transmitted wave $\overrightarrow{E^t}$ can be characterized by linear polarization components in the x and y directions:

$$\overrightarrow{E_+^{in}} = E_0\left(\hat{x} + j\hat{y}\right)e^{jk_0 z}e^{j\omega t} \tag{1}$$

$$\overrightarrow{E^t} = E_0\left(T_x\hat{x} + jT_y\hat{y}\right)e^{jk_0 z}e^{j\omega t} \tag{2}$$

where E_0 is the electric field strength, $k_0 = 2\pi/\lambda$ the wave number in free space, and $\omega = 2\pi f$ the angular frequency. When the transmission amplitude of the two orthogonal components is close to 1 ($T_x = 1 \cdot e^{j\varphi_x}$, $T_y = 1 \cdot e^{j\varphi_y}$), and the phase difference is 180° ($\varphi_x - \varphi_y = 180°$), the expression of the transmitted wave can be written as:

$$\overrightarrow{E_-^t} = E_0\left(\hat{x} - j\hat{y}\right)e^{j\varphi_x}e^{jk_0 z}e^{j\omega t} \tag{3}$$

At this time, the transmitted wave is converted from a left-handed circularly polarized wave to a right-handed circularly polarized wave. The geometric phase of the unit cell is realized by rotating the patch around the z-axis by the angle θ. The transmission Jones matrix of the unit cell before rotation can be expressed as $T(0) = \begin{pmatrix} t_{xx} & t_{xy} \\ t_{yx} & t_{yy} \end{pmatrix}$, and after the rotation, the Jones matrix changes to $T(\theta) = M \cdot T \cdot M^{-1}$. Matrix $M = \begin{pmatrix} \cos\theta & \sin\theta \\ -\sin\theta & \cos\theta \end{pmatrix}$ represents the conversion between the local coordinate system and global coordinate system, and the transmitted electromagnetic field can be expressed as:

$$\begin{pmatrix} E_+^t \\ E_-^t \end{pmatrix} = \begin{pmatrix} \frac{1}{2}\left[t_{xx}+t_{yy}+j\left(t_{xy}-t_{yx}\right)\right] & \frac{1}{2}\exp\left(j2\theta\right)\left[t_{xx}-t_{yy}-j\left(t_{xy}+t_{yx}\right)\right] \\ \frac{1}{2}\exp\left(-j2\theta\right)\left[t_{xx}-t_{yy}+j\left(t_{xy}+t_{yx}\right)\right] & \frac{1}{2}\left[t_{xx}+t_{yy}-j\left(t_{xy}-t_{yx}\right)\right] \end{pmatrix} \begin{pmatrix} E_+^{in} \\ E_-^{in} \end{pmatrix} \tag{4}$$

It can be seen that when the incident wave is left-handed circular polarization, the additional phase φ_- of the transmitted beam is -2θ, which is twice the geometric rotation angle of the unit cell structure. When the incident wave is right-handed circular polarization, the additional phase φ_+ is 2θ, which is also twice the geometric rotation angle of the unit cell structure, but the change trend is opposite.

The electromagnetic simulation software CST 2019 is used to model and analyze the unit cell. The boundary condition is set as the periodic boundary, and the port is set as the Floquet port whose electric field polarization directions of the two modes are x and y directions, respectively. When the

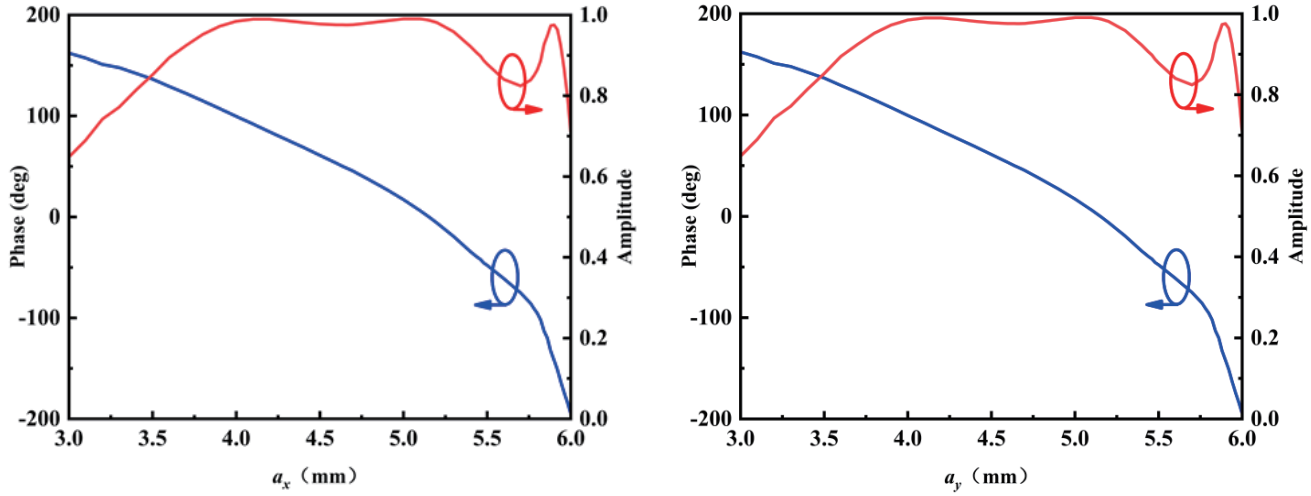

Figure 2. The transmission phase and amplitude of the unit cell (a) changed with a_x when the incident wave is x-polarization, (b) changed with a_y when the incident wave is y-polarization.

polarization direction of the incident wave is the x direction, a_y remains unchanged at 4 mm, and the relationship between the transmission phase and amplitude of the unit cell at 15 GHz and the cross patch parameter a_x is shown in Figure 2(a). Similarly, the transmission phase and amplitude of the unit cell is shown in Figure 2(b) when the wave polarization direction is the y direction. The phase coverage of the unit cell in the two orthogonal polarization directions reaches 360°. The transmission coefficient is higher than 85%, and the change of any arm length only affects the phase and amplitude responses of the corresponding polarization direction.

In order to realize the polarization conversion of the circularly polarized incident wave, it is necessary to keep the phase difference of the two orthogonal linear polarization components of the unit cell at 180°. Four unit cells with a phase gradient of 90° in two orthogonal polarization directions are selected to meet the requirements of resonance phase control, with a_x being 5.88 mm, 5.5 mm, 4.68 mm, 3.5 mm, and corresponding a_y being 4.68 mm, 3.5 mm, 5.88 mm, 5.5 mm, as shown in Figure 3. In 13–17 GHz, the transmission phase of the selected 4 types of unit cells varies with frequency graphs as shown in Figure 4. The phase difference between the two orthogonal components of each unit cell is 180°, and the phase difference with the adjacent unit cell in any polarization direction is 90°.

Geometric phase control can be used to design a unit cell sensitive to circular polarization. The

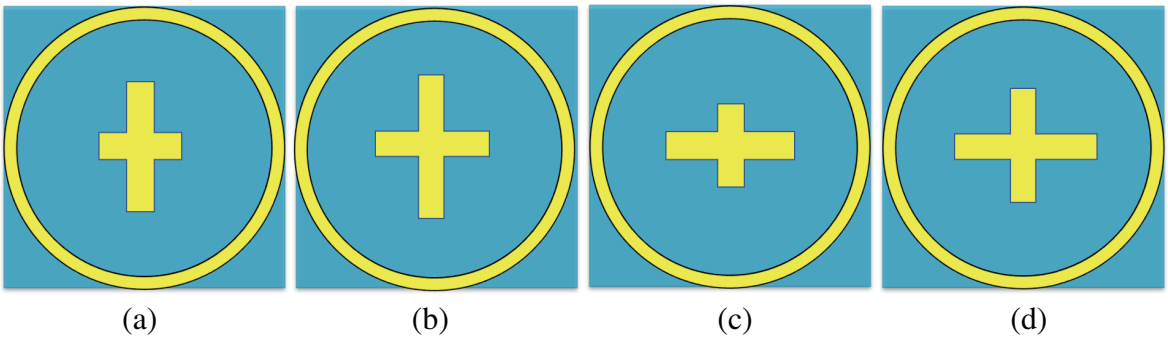

Figure 3. Schematic diagram of the 4 types of unit cell structures. (a) unit cell 1, (b) uint cell 2, (c) unit cell 3, (d) unit cell 4.

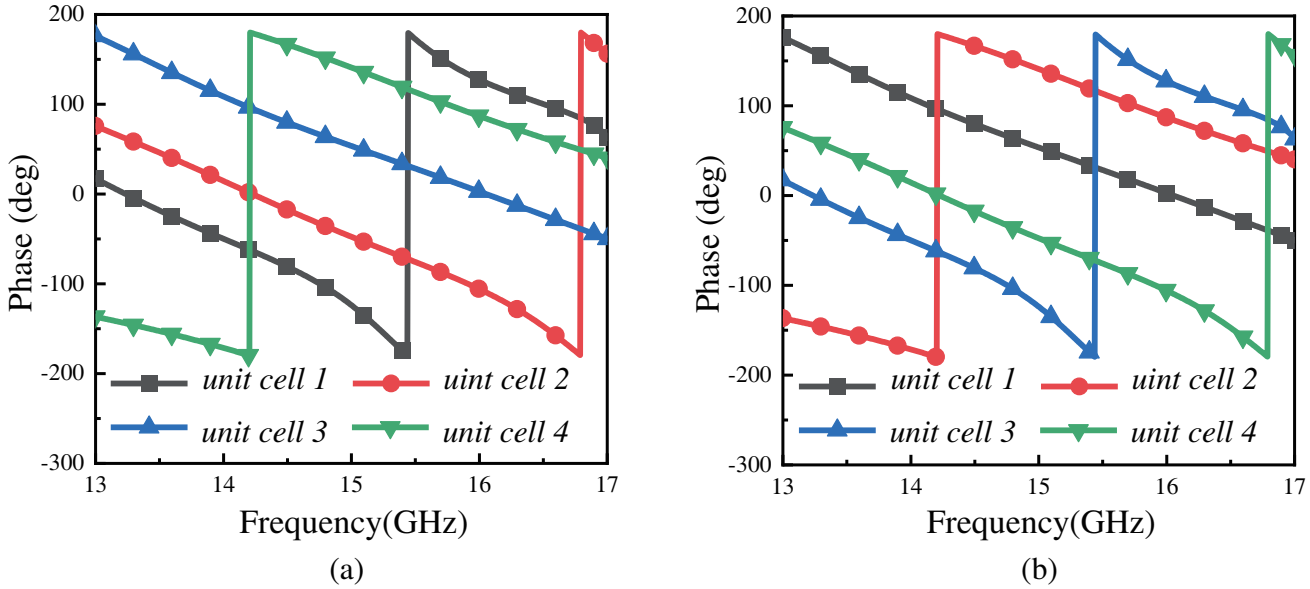

Figure 4. Curve of transmission phase versus frequency when electromagnetic waves are incident in different polarization directions (a) x-polarization (b) y-polarization.

specific method is to make the phase response of the unit cell to the x-polarized incident wave and the phase response to the y-polarized incident wave differ by 180°, by rotating the patch θ around the z axis, so as to get a geometric phase of 2θ. For unit cell (a), in 13–17 GHz, when linearly polarized waves are incident, the phase and amplitude responses of the unit cell are shown in Figure 5(a) and Figure 5(b). The difference between the phase response of the x-polarized incident wave and the phase response of the y-polarized incident wave is maintained at about 180°. When the operating frequency is 15 GHz, the amplitude response of the two orthogonal polarization directions is greater than 0.85, which is close to 1. When a left-handed circularly polarized wave is incident, the PCR of the unit cell is shown in Figure 5(c). At the center frequency of 15 GHz, the PCR is greater than 0.9. When circularly polarized waves are incident with different rotation directions, the relationship between the phase response of the unit cell and the rotation angle of the patch is shown in Figure 6. It can be seen that the patch rotates θ around the z axis, and the value of the unit cell phase response changes to 2θ.

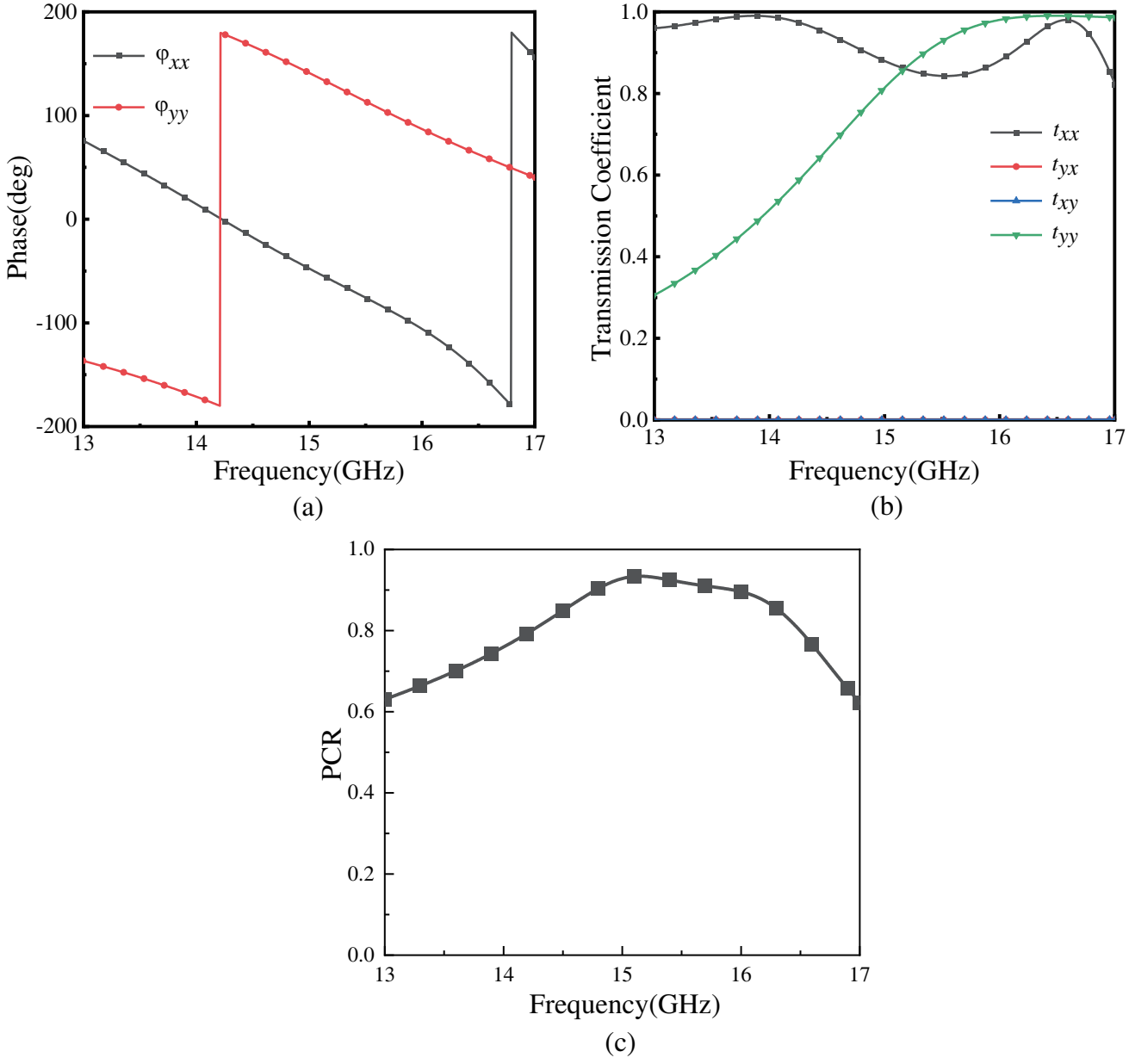

Figure 5. Characteristics of the unit cell 4. (a) Phase response. (b) Amplitude response. (c) PCR.

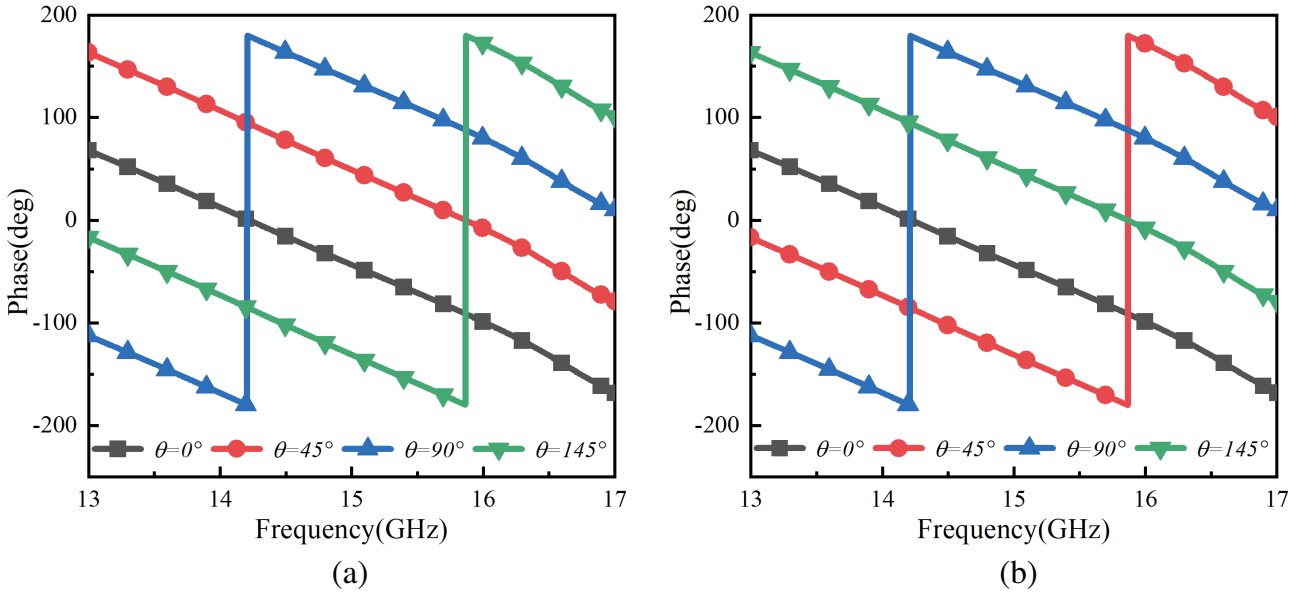

Figure 6. The phase response of the unit cell by rotating θ when electromagnetic waves are incident in different polarization directions (a) left-handed circular polarization (b) right-handed circular polarization.

3. DESIGN OF ARRAY

Controlling circularly polarized waves through resonance phase is essentially achieved by controlling two orthogonal linear polarized components with a phase difference of 180°. It has the same controlling effect for incident waves of any rotation direction. When the circularly polarized wave is controlled by geometric phase, the left-handed circularly polarized phase response and right-handed circularly polarized phase response are obtained by rotating the unit cell. When the unit cell rotation angle is fixed, its phase response is also fixed, so it can only control the incident wave in a specific direction of rotation. Combining resonant phase control and geometric phase control, the phase distribution of the left-handed circularly polarized beam and right-handed circularly polarized beam can be independently designed to achieve different effects, as shown in Figure 7.

The left-handed circularly polarized beam and right-handed circularly polarized beam that are perpendicularly incident on the metasurface are divided into two transmitted beams with different propagation directions, and the polarization direction is orthogonal to the incident wave. The entire metasurface array can be expressed by the transmission Jones matrix $T(x,y)$ [17]:

$$T(x,y) = \begin{bmatrix} \dfrac{\exp[i\varphi_L(x,y)] + \exp[i\varphi_R(x,y)]}{2} & \dfrac{i\exp[i\varphi_R(x,y)] - i\exp[i\varphi_L(x,y)]}{2} \\ \dfrac{i\exp[i\varphi_R(x,y)] - i\exp[i\varphi_L(x,y)]}{2} & \dfrac{-\exp[i\varphi_L(x,y)] - \exp[i\varphi_R(x,y)]}{2} \end{bmatrix} \tag{5}$$

where $\varphi_L(x,y)$ represents the phase distribution of left-handed circular polarization, and $\varphi_R(x,y)$ represents the phase distribution of right-handed circular polarization. Combining the principles of resonance phase and geometric phase, extracting the phase information in formula (5), after sorting it out, we can get [17]:

$$\varphi_x(x_i,y_j) = [\varphi_L(x_i,y_j) + \varphi_R(x_i,y_j)]/2 \tag{6}$$

$$\varphi_y(x_i,y_j) = [\varphi_L(x_i,y_j) + \varphi_R(x_i,y_j)]/2 - \pi \tag{7}$$

$$\theta(x_i,y_j) = [\varphi_L(x_i,y_j) - \varphi_R(x_i,y_j)]/4 \tag{8}$$

In the above formula, (x_i,y_j) represents the center position of the unit cell in the i-th row and j-th column on the metasurface array. $\varphi_x(x_i,y_j)$ and $\varphi_y(x_i,y_j)$ represent the phase of the unit cell at

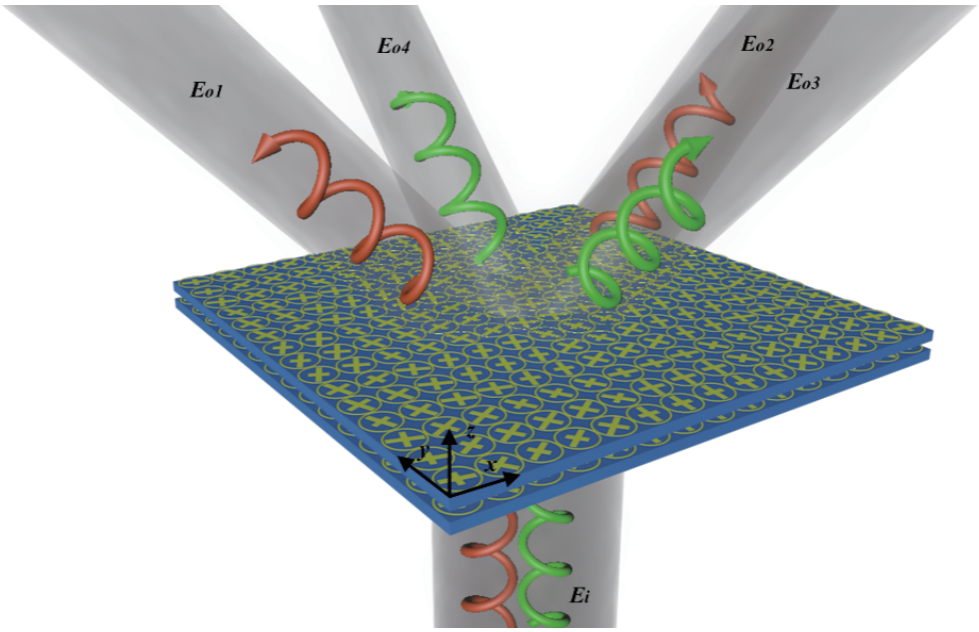

Figure 7. Schematic diagram of circular polarization multiplexing beam splitter.

the point in the two orthogonal polarization directions of x and y, that is, the resonance phase, and $\theta(x_i, y_j)$ represents the angle of rotation of the unit cell patch at the point, that is, the geometric phase. $\varphi_L(x_i, y_j)$ and $\varphi_R(x_i, y_j)$ respectively represent the phase distributions of the transmitted left-handed circularly polarized wave and right-handed circularly polarized wave. According to formulas (6)–(8), the structural parameters and rotation angle of each element on the metasurface array can be calculated. According to the principle of electric field superposition [18], the phase distribution of two right-handed circularly polarized beams is separated on the plane of Phi = 0°, and the phase distributions of two left-handed circularly polarized beams are separated on the plane of Phi = 90°:

$$\varphi_L(x_i, y_j) = \mathrm{mod}\{\arg[\exp(-jk_0d)] - \arg\{[\exp(jk_0f_1) + \exp(jk_0f_2)]\}, 2\pi\} \quad (9)$$

$$\varphi_R(x_i, y_j) = \mathrm{mod}\{\arg[\exp(-jk_0d)] - \arg\{[\exp(jk_0f_3) + \exp(jk_0f_4)]\}, 2\pi\} \quad (10)$$

In the formula, d represents the position vector where the feed source is located, and f represents the position vector of a point in the center direction of the preset transmitted beam. In this paper, d is set as (0, 0, −60 mm), f_1, f_2, f_3, f_4 is (40 mm, 0,60 mm), (−40 mm, 0,60 mm), (0,30 mm, 60 mm), (0, −30 mm, 60 mm), respectively.

The feed antenna is a microstrip patch antenna, and the feeding method is back feed. Degenerate mode separation is achieved by cutting the corner of the patch. The left-handed and right-handed circularly polarized antennas are simulated and modeled in the CST. When the working frequency is 15 GHz, when Phi = 0°, the axial ratio of the left-handed circularly polarized antenna is 0.12 dB, and the axial ratio of the right-handed circularly polarized antenna is 0.22 dB, which meets the feed demand. The simulation and processing test results are shown in Figure 8.

Formulas (9) and (10) can be used to calculate the phase distribution of the left-handed circular polarization and right-handed circular polarization beams. The discrete linear polarization phase distribution diagrams are shown in Figures 9(a) and (b). The rotation angle is shown in Figure 9(c) after converting the phase of each point to the corresponding size parameter, and the array model is shown in Figure 9(d).

Under open boundary conditions, the left-handed circularly polarized antenna and right-handed circularly polarized antenna are used as feed sources, and the beam splitter array is jointly simulated with time domain solver in CST. The three-dimensional far-field scattering pattern obtained by the time domain solver is shown in Figure 10.

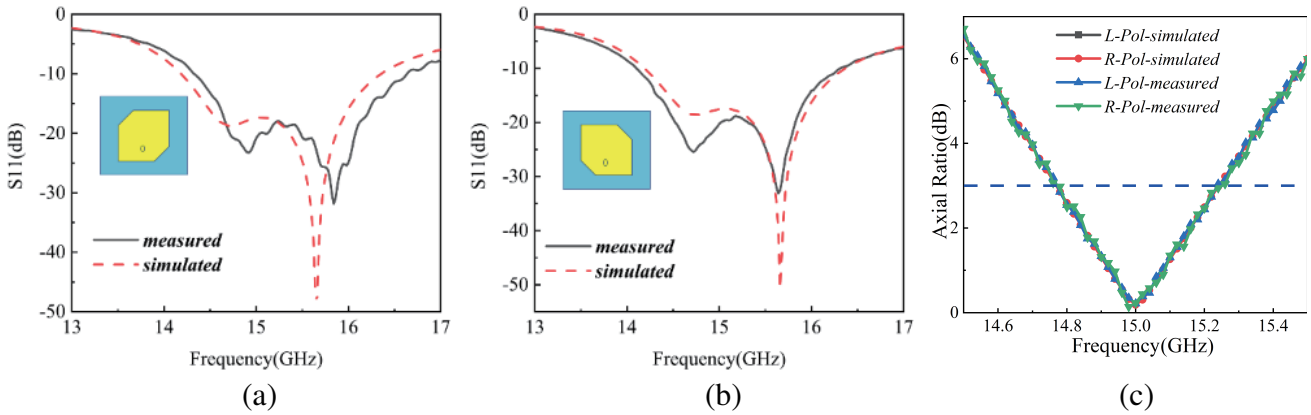

Figure 8. Schematic diagram and the characteristic parameters of the feed antenna (a) left-handed circular polarization (b) right-handed circular polarization (c) axial ratio.

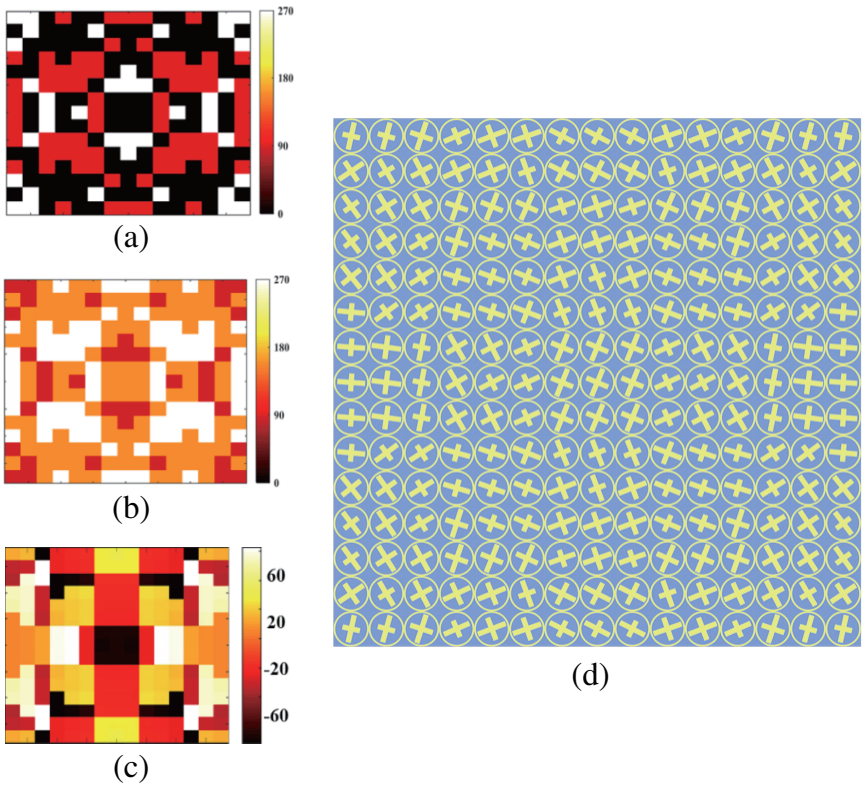

Figure 9. Schematic diagram of phase distribution and array model (a) x-polarization phase distribution (b) y-polarization phase distribution (c) rotation angle distribution (d) array model.

When the incident wave is left-handed circular polarization, the transmitted beam is divided into two right-handed circularly polarized beams with exit angles of $-33°$ and $33°$ on the xoz plane; when the incident wave is right-handed circular polarization, the transmitted beam is divided into two left-handed circularly polarized beams with exit angles of $-26°$ and $26°$ on the yoz plane.

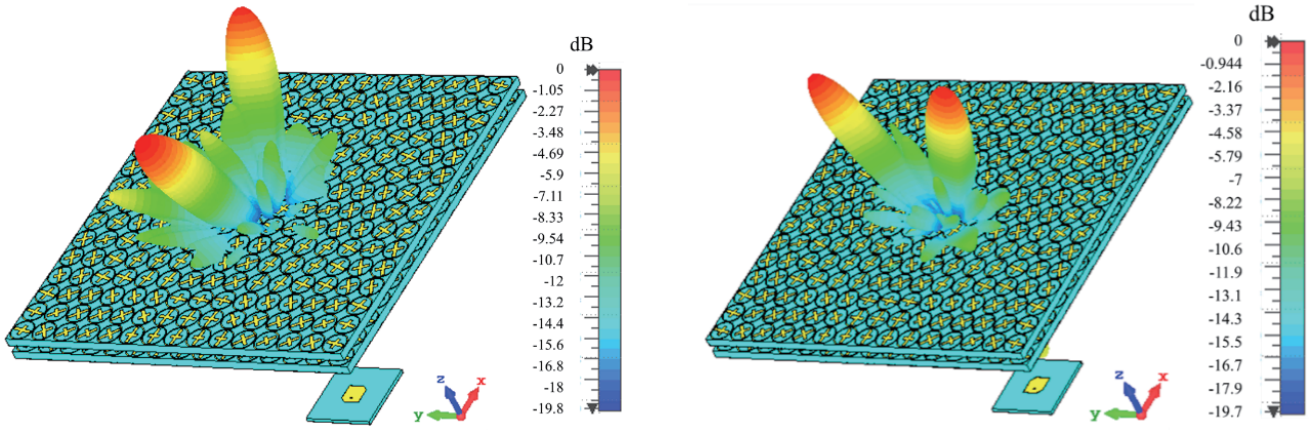

(a) (b)

Figure 10. Three-dimensional far-field scattering pattern of different circularly polarized waves incident(a) left-handed circular polarization (b) right-handed circular polarization.

Table 1. Contrast to previous designs.

Ref.	Center Wavelength	Polarization conversion ratio	Beam splitting angle (LCP)	Beam splitting angle (RCP)	Number of beams
[19]	1350 nm	90%	22.4°	−22.4°	2
[20]	27 mm	90%	−43°	43°	2
[21]	300 µm	—	−30°	30°	2
[22]	30 mm	—	−25°	25°	2
[23]	857 µm	—	45°	45°	2
[24]	532 nm	—	−24°,24°	−24°,24°	4
This paper	20 mm	90%	−33°,33°	−26°,26°	4

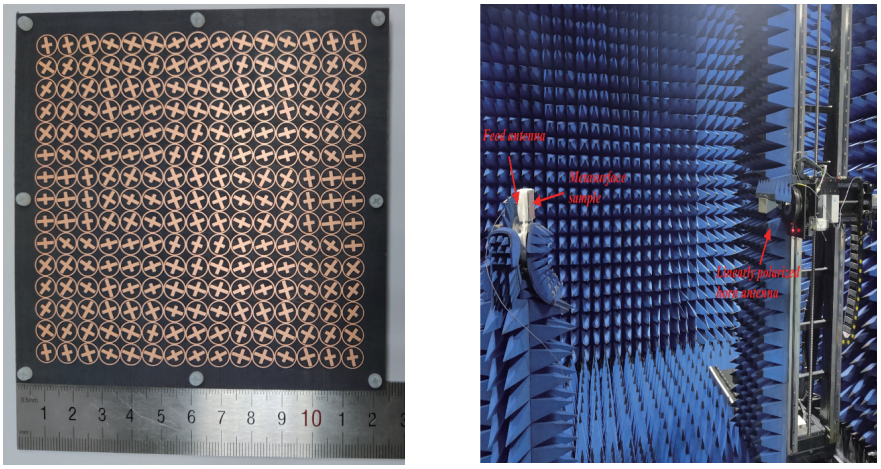

(a) (b)

Figure 11. Diagram of sample and test scene (a) sample (b) test scene.

4. TESTING AND DISCUSSION

In order to verify the performance of the designed circular polarization metasurface beam splitter, a sample of the beam splitter with a size of 119 mm ∗ 119 mm was fabricated through PCB processing, as shown in Figure 11(a). In order to reduce the impact of environmental noise, a test platform as shown in Figure 11(b) was built in a microwave anechoic chamber. The linear polarization horn was placed on the console, and the electric field of two orthogonal linear polarization components were measured at the operating frequency of 15 GHz. The calculated left-handed and right-handed circular polarization far-field scattering patterns and axis ratios are shown in Figure 12 and Figure 13.

As shown in Figure 12, when a left-handed circularly polarized patch is used as a feed source, two

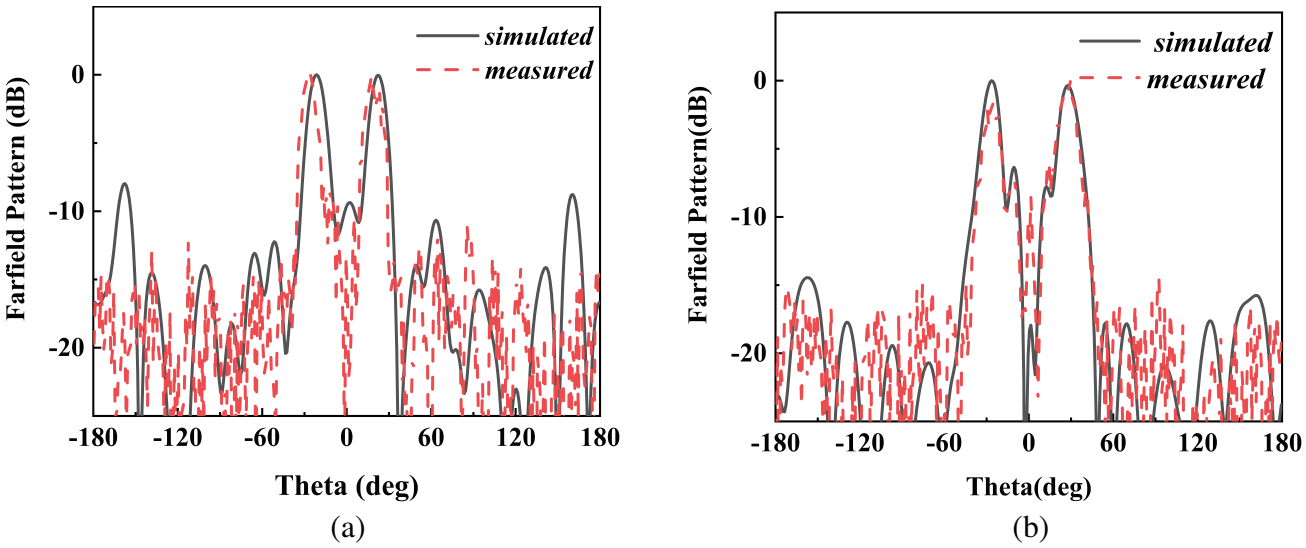

Figure 12. Cartesian pattern of different circularly polarized incident waves (a) right-handed circularly polarized wave, Phi = 90° (b) left-handed circularly polarized wave, Phi = 0°.

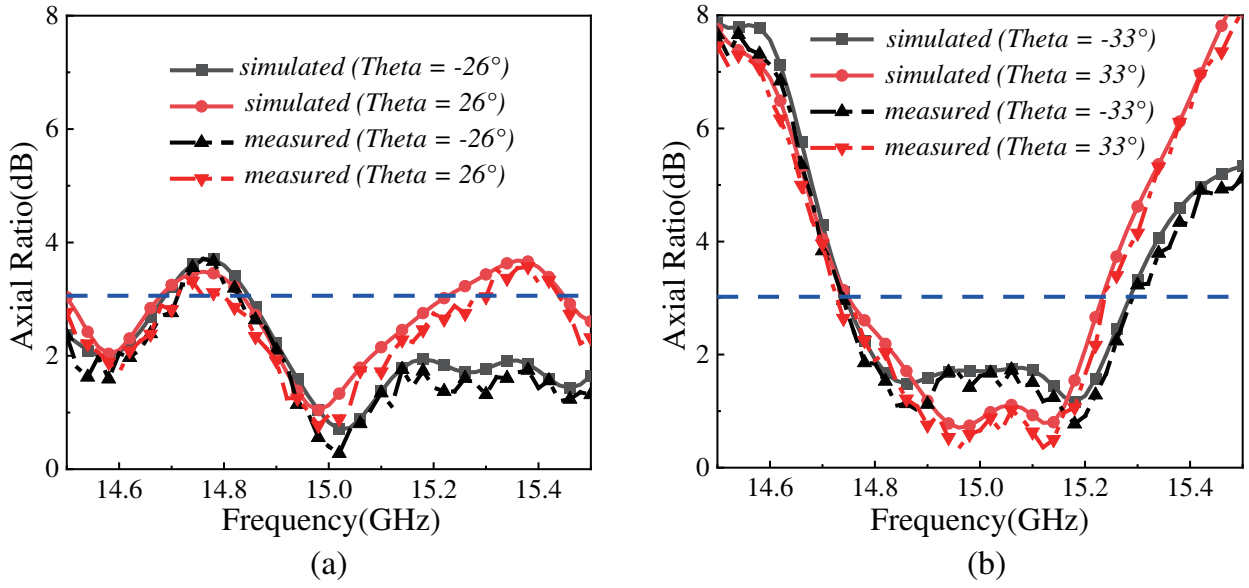

Figure 13. Axial ratio when different circularly polarized waves are incident (a) right-handed circularly polarized wave, Phi = 90° (b) left-handed circularly polarized wave, Phi = 0°.

right-handed circularly polarized waves with propagation directions of -33° and 33° are obtained on the plane of Phi= 0°. When a right-handed circularly polarized patch is used as a feed source, two left-handed circularly polarized waves with propagation directions of -26° and 26° are obtained on the plane of Phi = 90°. Within the 3 dB axial ratio bandwidth of the patch antenna, the axial ratios of the four transmitted beams in the center direction are all less than 3 dB, and the polarization conversion efficiency is greater than 90%. The experimental results are consistent with the simulation ones. The metasurface beam splitter can convert circularly polarized incident waves into orthogonal circularly polarized waves. Our work is compared with previous designs, as shown in Table 1. While separating the circularly polarized components in the incident wave, we perform a beam splitting operation on the transmission beam. The polarization conversion ratio at 15 GHz is greater than 90%, and the effect of transmission wave splitting in each polarization direction is different.

5. CONCLUSION

In this paper, we have designed and processed a sub-wavelength thickness circular polarization multiplexing metasurface beam splitter, which integrates the functions of polarization conversion and polarization beam splitting. By combining the principle of resonance phase and geometric phase control, the decoupling of the phase distributions of left-handed circular polarization and right-handed circular polarization is realized, so that the array has different beam splitting effects for left-handed circular polarization and right-handed circular polarization incident waves. The polarization conversion ratio is higher than 90%. Simulated and experimental results show that the metasurface circular polarization beam splitter can achieve excellent beam splitting effects while changing the polarization direction of the incident wave. This work has potential applications in the fields of anisotropic devices, beam scanning, and wireless communication systems.

REFERENCES

1. Zhang, L., J. Guo, and T. Ding, "Ultrathin dual-mode vortex beam generator based on anisotropic coding metasurface," *Scientific Reports*, Vol. 11, No. 1, Art. No. 5766, Mar. 11, 2021.
2. Zhang, Z., Y. Zhang, T. Wu, S. Chen, W. Li, and J. Guan, "Broadband RCS reduction by a quaternionic metasurface," *Materials*, Vol. 14, No. 11, Art. No. 2787, Jun. 2021.
3. Ali, L., Q. Li, T. A. Khan, J. Yi, and X. Chen, "Wideband RCS reduction using coding diffusion metasurface," *Materials*, Vol. 12, No. 17, Art. No. 2708, Sep 2019.
4. Yu, Y., F. Xiao, I. D. Rukhlenko, and W. Zhu, "High-efficiency ultra-thin polarization converter based on planar anisotropic transmissive metasurface," *Aeu-International Journal of Electronics and Communications*, Vol. 118, Art. No. 153141, May 2020.
5. Fan, J. and Y. Cheng, "Broadband high-efficiency cross-polarization conversion and multi-functional wavefront manipulation based on chiral structure metasurface for terahertz wave," *Journal of Physics D — Applied Physics*, Vol. 53, No. 2, Art. No. 025109, Jan. 9, 2020.
6. Chen, L., Q. F. Nie, Y. Ruan, and H. Y. Cui, "Anisotropic metasurface with high-efficiency reflection and transmission for dual-polarization," *Applied Physics A — Materials Science & Processing*, Vol. 126, No. 9, Art. No. 758, Sep. 1, 2020.
7. Wu, L. W., H. F. Ma, R. Y. Wu, Q. Xiao, Y. Gou, M. Wang, Z. X. Wang, L. Bao, H. L. Wang, Y. M. Qing, and T. J. Cui, "Transmission-reflection controls and polarization controls of electromagnetic holograms by a reconfigurable anisotropic digital coding metasurface," *Advanced Optical Materials*, Vol. 8, No. 22, Art. No. 2001065, Nov. 2020.
8. Bao, Y., J. Yan, X. Yang, C.-W. Qiu, and B. Li, "Point-source geometric metasurface holography," *Nano Letters*, Vol. 21, No. 5, 2332–2338, Mar. 10, 2021.
9. Yoon, G., D. Lee, K. Nam, and J. Rho, "Geometric metasurface enabling polarization independent beam splitting," *Scientific Reports*, Vol. 8, Art. No. 9468, Jun. 21, 2018.
10. Umul, Y. Z., "Diffraction of electromagnetic waves by a planar interface between perfectly absorbing and anomalously transmitting metasurface half-planes," *Optik*, Vol. 179, 173–181, 2019.

11. Maguid, E., I. Yulevich, M. Yannai, V. Kleiner, M. L. Brongersma, and E. Hasman, "Multifunctional interleaved geometric-phase dielectric metasurfaces," *Light-Science & Applications*, Vol. 6, Art. No. e17027, Aug. 11, 2017.
12. Liu, S., T. J. Cui, Q. Xu, D. Bao, L. L. Du, X. Wan, W. X. Tang, C. M. Ouyang, X. Y. Zhou, H. Yuan, H. F. Ma, W. X. Jiang, J. G. Han, W. L. Zhang, and Q. Cheng, "Anisotropic coding metamaterials and their powerful manipulation of differently polarized terahertz waves," *Light-Science & Applications*, Vol. 5, Art. No. e16076, May 2016.
13. Lv, B. Y., C. M. Ouyang, H. F. Zhang, Q. Xu, Y. F. Li, X. Q. Zhang, Z. Tian, J. Q. Gu, L. Y. Liu, J. G. Han, and W. L. Zhang, "All-dielectric metasurface-based quad-beam splitter in the terahertz regime," *Ieee Photonics Journal*, Vol. 12, No. 5, Art. No. 4601410, Oct. 2020.
14. Ding, X., L. Zhang, K. Zhang, Q. Wu, and C.-W. Qiu, "Ultrathin metasurface based on phase discontinuity with maximal cross-polarization efficiency," *IEEE MTT-S International Microwave Workshop Series on Advanced Materials and Processes for RF and THz Applications (IEEE MTT-S IMWS-AMP 2015)*, 266–268, Suzhou, China, 2015.
15. Ding, X. M., F. Monticone, K. Zhang, L. Zhang, D. L. Gao, S. N. Burokur, A. de Lustrac, Q. Wu, C.-W. Qiu, and A. Alu, "Ultrathin pancharatnam-berry metasurface with maximal cross-polarization efficiency," *Advanced Materials*, Vol. 27, No. 7, 1195–1200, Feb. 18, 2015.
16. Mueller, J. P. B., N. A. Rubin, R. C. Devlin, B. Groever, and F. Capasso, "Metasurface polarization optics: Independent phase control of arbitrary orthogonal states of polarization," *Physical Review Letters*, Vol. 118, No. 11, Art. No. 113901, Mar. 14 2017.
17. Liu, M. Z., P. C. Huo, W. Q. Zhu, C. Zhang, S. Zhang, M. W. Song, S. Zhang, Q. W. Zhou, L. Chen, H. J. Lezec, A. Agrawal, Y. Q. Lu, and T. Xu, "Broadband generation of perfect Poincare beams via dielectric spin-multiplexed metasurface," *Nature Communications*, Vol. 12, No. 1, Art. No. 2230, Apr. 13, 2021.
18. Pang, H., H. Gao, Q. Deng, S. Yin, Q. Qiu, and C. Du, "Multi-focus plasmonic lens design based on holography," *Optics Express*, Vol. 21, No. 16, 18689–18696, Aug. 12, 2013.
19. Chen, M., D. P. Zhao, J. J. Cai, C. Y. Wang, X. F. Xiao, and L. Z. Chang, "All-dielectric metasurfaces for circularly polarized beam-splitters with high conversion efficiency and broad bandwidth," *Optik*, Vol. 165, 41–49, 2018.
20. Lee, W. S. L., S. Nirantar, D. Headland, M. Bhaskaran, S. Sriram, C. Fumeaux, and W. Withayachumnankul, "Broadband terahertz circular-polarization beam splitter," *Advanced Optical Materials*, Vol. 6, No. 3, 1700852, 2018.
21. Liu, C. B., Y. Bai, Q. Zhao, Y. H. Yang, H. S. Chen, J. Zhou, and L. J. Qiao, "Fully controllable pancharatnam-berry metasurface array with high conversion efficiency and broad bandwidth," *Scientific Reports*, Vol. 6, 34819, 2016.
22. Xie, X., M. B. Pu, K. P. Liu, X. L. Ma, X. Li, J. N. Yang, and X. G. Luo, "High-efficiency and tunable circular-polarization beam splitting with a liquid-filled all-metallic catenary meta-mirror," *Advanced Materials Technologies*, Vol. 4, No. 7, 1900334, 2019.
23. Kuznetsov, S. A., V. A. Lenets, M. A. Tumashov, A. D. Sayanskiy, P. A. Lazorskiy, P. A. Belov, J. D. Baena, and S. B. Glybovski, "Self-complementary metasurfaces for designing terahertz deflecting circular-polarization beam splitters," *Applied Physics Letters*, Vol. 118, No. 13, 131601, 2021.
24. Yoon, G., D. Lee, K. Nam, and and J. Rho, "Geometric metasurface enabling polarization independent beam splitting," *Scientific Reports*, Vol. 8, 9468, 2018.